

This discussion paper is/has been under review for the journal Atmospheric Measurement Techniques (AMT). Please refer to the corresponding final paper in AMT if available.

# A method for sizing submicrometer particles in air collected on formvar films and imaged by scanning electron microscope

E. Hamacher-Barth<sup>1</sup>, K. Jansson<sup>2</sup>, and C. Leck<sup>1</sup>

<sup>1</sup>Department of Meteorology, Stockholm University, Stockholm, Sweden

<sup>2</sup>Department of Materials and Environmental Chemistry, Stockholm University, Stockholm, Sweden

Received: 21 May 2013 – Accepted: 27 May 2013 – Published: 19 June 2013

Correspondence to: E. Hamacher-Barth (evelyne@misu.su.se)

Published by Copernicus Publications on behalf of the European Geosciences Union.

## A method for sizing submicrometer particles in air

E. Hamacher-Barth et al.

Title Page

Abstract

Introduction

Conclusions

References

Tables

Figures

⏪

⏩

◀

▶

Back

Close

Full Screen / Esc

Printer-friendly Version

Interactive Discussion



## Abstract

Here we present a method to systematically investigate single aerosol particles collected on formvar film supported by a copper grid, with Scanning Electron Microscopy (SEM) operating at low accelerating voltage. The method enabled us to observe the surface of the sample grid at high resolution. Subsequent processing of the images with digital image analysis provided a statistically and quantitative size resolved information on the particle population including their morphology on the film. The quality of the presented method was established using polystyrene nanospheres as standards in the size range expected for ambient aerosol particles over remote marine areas (20–900 nm in diameter). The sizing was found to be critically dependent on the contrasting properties of the particles towards the collection substrate. The relative standard deviation of the diameters of polystyrene nanospheres was better than 10 % for sizes larger than 40 nm and 18 % for 21 nm particles compared with the manufacturer's certificate.

The size distributions derived from the microscope images of airborne aerosols collected during a research expedition to north of 80° N in the summer of 2008 were compared with simultaneously collected number particle size distributions seen by a Twin Differential Mobility Particle Sizer. We captured a representative fraction of the aerosol particles with SEM and were able to causally relate the determined morphological properties of the aerosol under investigation to aerosol transformation processes in air being advected from the marginal ice edge/open sea south of 80° N.

## 1 Introduction

Aerosol particles are ubiquitous in the troposphere and have a major influence on global climate and climate change. The direct influence of particles on climate is through scattering and absorption of both incoming light from space and thermal radiation emitted from Earth's surface. The indirect effect of airborne aerosols is related to their role as cloud condensation nuclei (CCN). The number, size, morphology and

AMTD

6, 5401–5446, 2013

### A method for sizing submicrometer particles in air

E. Hamacher-Barth et al.

Title Page

Abstract

Introduction

Conclusions

References

Tables

Figures



Back

Close

Full Screen / Esc

Printer-friendly Version

Interactive Discussion



## A method for sizing submicrometer particles in air

E. Hamacher-Barth et al.

Title Page

Abstract

Introduction

Conclusions

References

Tables

Figures

◀

▶

◀

▶

Back

Close

Full Screen / Esc

Printer-friendly Version

Interactive Discussion



chemical composition of the CCN will determine the number and size of the cloud drops and thus be important factors in determining the optical properties of clouds. The process of cloud formation however is still not fully understood and modeling these processes has a large degree of uncertainty, mainly due to a lack of observational data (IPCC, 2007). To improve our understanding of cloud droplet activation and evolution we need a much better understanding on how the chemistry of the aerosol multiphase system differs with size.

The atmosphere contains significant concentrations of aerosol particles with a diameter size span ranging from a few nanometers to around a few micrometers. It is therefore convenient to describe particle size with one single number. However, unless the particle is a perfect sphere, which is rare in natural atmospheric samples (Bigg and Leck, 2001), there are many ways, including shape/morphology, degree of compactness, state of mixture and particle texture, to describe an aerosol particle (Coz and Leck, 2011). The only method at present to derive size resolved mapping of single particles including the above parameters, down to sizes in the lower nanometer range, is electron microscopy (Coz et al., 2008; Coz and Leck, 2011; Laskin et al., 2006; Kandler et al., 2007; Capanelli et al., 2011; Leck and Bigg, 2008; Bigg et al., 2004).

When particles collected onto a thin film of carbon or polyvinyl formal (“formvar”), supported by a 3 mm transmission electron microscopy (TEM) copper grid, are imaged using the electron microscope the electron beam scatters more in the thicker and denser particulate material compared with the uniform grid film. The images usually have good contrast and excellent resolution in two dimensions. Three-dimensional (3-D) resolution of particles can be obtained by shading the grid surface film with deposited particles by fine metal coatings under a low angle (Bigg and Leck, 2001). However, by shadowing the particles they will end up being slightly larger in size which in turn will result in a false size number distribution and move the size limit of detection to larger sizes. Without shading, parts of the sample and the formvar film might on the other hand be destroyed by the high energy electron beam (80–200 kV) usually in operation.

## A method for sizing submicrometer particles in air

E. Hamacher-Barth et al.

Title Page

Abstract

Introduction

Conclusions

References

Tables

Figures

⏪

⏩

◀

▶

Back

Close

Full Screen / Esc

Printer-friendly Version

Interactive Discussion



Scanning electron microscopy (SEM) has been used for more than fifty years to image surfaces and particles (Junge, 1952; Parungo et al., 1986; Stevens et al., 2009) and can be operated at an accelerating voltage as low as 1 kV. This enables highly detailed imaging of beam sensitive particles without radiation damage, and in abandonment of metal coating information on size, morphology and chemical (elemental) composition is available without any distortion from any additional chemical constituent. Particle size and morphological parameters can be resolved down to 2–5 nm in diameter while chemical mapping can be made down to about 50–100 nm in diameter, but at a higher accelerating voltage. In any case, microscopic methods are not completely quantitative, and obtaining statistical information on an aerosol population is very time consuming. The availability of an objective and quantitative method for the evaluation of aerosol samples and microscope images is therefore a prerequisite for a systematic investigation. Moreover, to assess the net aerosol effects on cloud formation and regional climate it has to be assured that the aerosol samples form a representative fraction of the collected ambient aerosol.

Here we present a quantitative method to systematically investigate single aerosol particles collected on formvar film supported by a copper grid, with a SEM operating at low accelerating voltage. The method enables us to observe the surface of the sample grid at high resolution. Subsequent processing of the images with digital image analysis has provided statistically size resolved information on the particle population collected on the film. The use of certified polystyrene latex sphere standards to be used in calibration of surface screening inspection systems is discussed. Furthermore, the size distributions derived from evaluating microscope images of the spheres and natural samples were compared with simultaneously collected number particle size distributions seen by a Twin Differential Mobility Particle Sizer (TDMPS; Heintzenberg et al., 2012). Some of the problems associated with the size determination of natural samples are identified and discussed.

## 2 Methods for image recording and digital analysis

### 2.1 Scanning Electron Microscopy (SEM)

The samples were investigated with a high-resolution SEM (JEOL JSM-7401F) under high vacuum conditions, less than  $9.63 \times 10^{-5}$  Pa (Stevens, 2009). The electron beam was generated by a cold field emission gun operating with an extracting voltage of 6.8 kV yielding an emission of 20  $\mu$ A. The focused electron probe current was 16 pA and secondary electrons emitted from the sample surface were detected with an “in-lens” column detector. A negative bias (–2 kV) was applied to the sample stage to decelerate incident electrons before entering the sample surface. To generate a landing energy corresponding to 1 kV a column accelerating voltage of 3 kV was used. This so called Gentle Beam mode was used to minimize radiation damage, surface charge-up and electron beam diameter. Images were recorded after correction of stigmatism, focusing and automatic grey scale adjustment (contrast and brightness). Particle samples under investigation were collected directly onto 3 mm TEM copper 300 mesh grids, coated with a 30–60 nm thick formvar film (TED PELLA INC.).

### 2.2 Grid screening protocol

With the purpose to objectively photograph the particle population collected on the formvar film, each grid was screened systematically. To achieve this each grid was divided into four quadrants using the grid marker in the center of the grids, as displayed in Fig. 1a. The screening of a grid started from the grid marker and went outwards towards the edge of the grid following a quadrant’s (a, b, c or d) diagonal (i.e. 1,1; 2,2; 3,3, etc). In total between 7 and 9 squares were scanned, and between 300 and 500 images were obtained for each grid. To reduce the screening time and to obtain a sufficient number of images for digital image analysis the scanning of the grid started from a low magnification (80 $\times$ ). The whole grid was scanned in order to determine the orientation and to identify damaged areas, and proceeded via magnification of 1100 $\times$

## A method for sizing submicrometer particles in air

E. Hamacher-Barth et al.

Title Page

Abstract

Introduction

Conclusions

References

Tables

Figures

◀

▶

◀

▶

Back

Close

Full Screen / Esc

Printer-friendly Version

Interactive Discussion



to take an image of a square in the copper grid, and finally images at 10000× and 40000× were recorded (Fig. 1). The latter were used in the digital imaging procedure.

## 2.3 Digital image analyses

Digital image analysis encompasses all processes that are necessary to extract information from a digital image: image processing, segmentation of the object (the aerosol particle) from the background, and measurement of the desired parameters. Microscope images at 40000× were evaluated using an optimized commercially available image processing software (Aphelion™ Dev 4.10). Quantitative description of a particle is often a more complex matter than it first appears and measuring particle size alone is sometimes insufficiently sensitive to identify subtle differences between single particles. In addition to size we therefore use morphological parameters to extend the description of the mapped particles (standards and natural samples). These descriptors (elongation and circularity) give a measure on the deviation from spherical geometry and can be directly addressed by the image processing software.

### 2.3.1 Separation of particles from the background

To reduce the background noise of the digital image obtained with SEM an Automedian filter and subsequently a Gauss filter (3 × 3) were applied to each image. The following separation of the imaged aerosol particles from their background requires the determination of the intensity of their neighbouring background. Therefore an image section of the particle background was produced at a size of about 250 × 250 pixels by cutting out the aerosol particle (Fig. 2 left, area inside the dashed rectangle) determining the maximal background intensity (see Fig. 2, left). Exactly the same image but including the aerosol particle enabled us to separate the particle and determine its area (in pixel; see Fig. 2, right) by setting 40 % of the intensity difference between background and aerosol maximal intensity as a threshold (see Fig. 3).

## A method for sizing submicrometer particles in air

E. Hamacher-Barth et al.

Title Page

Abstract

Introduction

Conclusions

References

Tables

Figures

◀

▶

◀

▶

Back

Close

Full Screen / Esc

Printer-friendly Version

Interactive Discussion



### 2.3.2 Particle size

The size of an aerosol particle can be expressed by calculating the diameter ( $D_{pa}$ ) of an equivalent sphere which covers the same area according to Eq. (1)

$$D_{pa} = \sqrt{\text{Area}/\pi} \quad (1)$$

$D_{pa}$  is the diameter of a sphere that comprises the same area as the projected dry vacuum particle. The value for the area is calculated from the number of pixels counted for each particle (Allen, 1997; Hinds, 1999).

From the particle area (in pixel) the diameter of an equivalent sphere for each aerosol particle was calculated according to Eq. (1). A number size distribution for the respective aerosol sample was obtained by calculating a histogram using MATLAB 2011a and the free available software package EasyFit.

### 2.3.3 Morphological properties

The morphological properties of the particles have been quantified by the following parameters:

- *Circularity* is sensitive to both overall form and surface roughness, showing values in the range from 0 until 1. A perfect circle has a circularity of 1 while a very irregular object has a circularity value closer to 0 (see Fig. 4).

$$\text{Circularity} = \frac{4\pi\text{Area}}{\text{CP}^2} \quad (2)$$

Circularity uses the Crofton perimeter (CP), which is calculated according to Eq. (3)

$$\text{CP} = \pi \sum_{i=1}^n N_i(X, k_i) \quad (3)$$

## A method for sizing submicrometer particles in air

E. Hamacher-Barth et al.

Title Page

Abstract

Introduction

Conclusions

References

Tables

Figures

◀

▶

◀

▶

Back

Close

Full Screen / Esc

Printer-friendly Version

Interactive Discussion



with  $N_i(X, \omega_i)$  the intercept of  $X$  in the orientation  $\omega_i$  and  $k_i$  coefficient to correct for the bias depending on the orientation of the particle on the image. Aphelion™ 4.10 uses 4 orientations ( $\omega = 0^\circ$ ,  $\omega_1 = 45^\circ$ ,  $\omega_2 = 90^\circ$  and  $\omega_3 = 135^\circ$ );  $k$  and  $k_2$  equal 1, whereas  $k_1$  and  $k_3$  equal  $1/\sqrt{2}$ . An intercept is the number of transitions from intensity to non-intensity in a given orientation (see Fig. 5; Meyer, 1990; Serra, 1988).

- *Elongation* is sensitive to the overall form of a particle and is calculated according to Eq. (4).

$$\text{Elongation} = \frac{(D_{\max} - D_{\min})}{(D_{\max} + D_{\min})} \quad (4)$$

$D_{\max}$  is the longest projection of the particle,  $D_{\min}$  is the shortest projection. Elongation shows values to zero and 1; for compact particles the value is closer to zero whereas for open branched ones elongation is closer to 1. The higher the ratio  $D_{\max}/D_{\min}$  the closer to 1 the value for elongation becomes (see Fig. 4); for a particle with  $D_{\max}/D_{\min} = 1000 : 1$  the elongation is calculated to 0.998.

### 3 Methods for sampling of airborne aerosol particles during ASCOS

The approach using scanning electron microscopy with subsequent image mapping described above (Sect. 2) and below (Sect. 4) was applied to two ambient aerosol samples (see Sect. 5.1 for details) collected onboard the Swedish icebreaker *Oden* in the course of the Arctic Summer Cloud Ocean Study (ASCOS) in 2008. ASCOS focused on the study of the formation and life cycle of low-level Arctic clouds with linkages to the microbiological life in ocean and ice. ASCOS departed from Longyearbyen on Svalbard on 2 August and returned on 9 September. After traversing the pack ice northward an ice camp was set up on 12 August at  $87^\circ$  N and remained in operation through 1 September, drifting with the ice. Tjernström et al. (2013) have documented

the ASCOS instrument suite in detail. Key methods for sampling used in this study are described below.

*The sampling manifold.* A  $\text{PM}_{10}$ -inlet (diameter  $< 10 \mu\text{m}$  at ambient relative humidity) was utilized upstream of all aerosol measurements located in a laboratory container on the 4th deck of the icebreaker. The aerosol inlet was designed to optimize the distance from the sea and from the ship's superstructure: located  $\sim 25 \text{m}$  above the sea surface, 3 m above the roof of the laboratory container. Direct contamination from the ship was excluded by using a pollution controller. Provided that the wind was within  $\pm 70^\circ$  of the direction of the bow and stronger than  $2 \text{ms}^{-1}$ , no pollution reached the sample inlets (Leck et al., 1996). To maximize the sampling time it was necessary to face the ship into the wind. More details of the set up for the sampling of aerosol particles are given in Leck et al. (2001).

*Collection of particles for subsequent single particle mapping by SEM.* Airborne aerosol particles were collected directly onto the formvar surfaces of the 3 mm TEM grids with an electrostatic precipitator as described earlier (Dixkens and Fissan, 1999; Leck and Bigg, 2008). In brief, particle charges were imparted at the aerosol inlet by a  $^{63}\text{Ni}$  beta-emitting radioactive source and particles were precipitated by a  $12 \text{kV cm}^{-1}$  electric field between the inlet and the collecting surface. Flow rate was kept very low ( $0.17 \text{mLs}^{-1}$ ) in order to collect particles up to  $\sim 1$  micrometer. The collection efficiency of the electrostatic precipitator was inter-compared with the TSI 1236 Nanometer Aerosol Sampler ( $^{63}\text{Ni}$  beta-emitting radioactive source and sample flow of  $1 \text{L m}^{-1}$ ) mounted side-by-side with the electrostatic precipitator. Both collected a small, but statistically significant number of particles  $< 25 \text{nm}$ . The precipitator took samples for 6 to 12 h. Before and after sampling the grids were placed in a gridholder box in a sealed dry plastic bag, together with silica gel packets, and stored in a desiccator at a constant temperature of  $20^\circ\text{C}$  before they were investigated.

*Number size distributions using a TDMPS.* The sampling system deployed to measure the number size distributions of dry sub-micrometer particles used pairs of differential mobility analyzers (DMAs). The TSI 3010 counters used in the DMAs were

## A method for sizing submicrometer particles in air

E. Hamacher-Barth et al.

Title Page

Abstract

Introduction

Conclusions

References

Tables

Figures

◀

▶

◀

▶

Back

Close

Full Screen / Esc

Printer-friendly Version

Interactive Discussion



## A method for sizing submicrometer particles in air

E. Hamacher-Barth et al.

Title Page

Abstract

Introduction

Conclusions

References

Tables

Figures

⏪

⏩

◀

▶

Back

Close

Full Screen / Esc

Printer-friendly Version

Interactive Discussion



size and concentration calibrated against an electrometer and the TSI 3025 counters for particle sizes below 20 nm diameter in the standard way (Stolzenburg, 1988). This set up yielded a complete number size distribution from 3 to 800 nm diameter in 45 intervals of diameter every 10 min. Further details of the TDMPMS system can be found in Heintzenberg and Leck (2012). Using NIST (National Institute of Standards Technology) traceable calibration standards of polystyrene latex (PSL) spherical particles the deviation in determination of the mobility diameter has been determined to  $\pm 5\%$  (W. Birmili, personal communication, 2013).

Number size distributions obtained from TDMPMS measurements were adapted to SEM measurements by taking the median value for each of the 45 TDMPMS size intervals by assuming the same particle diameter in the respective interval. The particle diameters were then merged to form a complete set of diameters across the TDMPMS measuring interval. The data were treated in the same way as the SEM derived data to obtain a number size distribution.

### 4 Polystyrene latex spheres used for SEM calibration

To determine the error on sizing with the SEM a range of NIST PSL spherical particles was investigated. The diameter values obtained with SEM/image mapping were compared with the values obtained by the manufacturer, and morphological parameters (circularity, elongation) were determined. The sizes of the standards were chosen to cover the size distribution of a remote marine atmospheric aerosol population in the submicrometer size range (Covert et al., 1996; Heintzenberg and Leck, 2012) as a superposition of more or less distinguishable modes, and we used PSL spheres of the following diameters:  $21 \pm 1$  nm,  $40 \pm 1$  nm,  $57 \pm 4$  nm,  $81 \pm 3$  nm,  $200 \pm 6$  nm, and  $903 \pm 12$  nm.

## 4.1 Sample preparation

To prepare the grid standards for subsequent screening and evaluation the bottle containing the microspheres (all polymer microsphere suspensions were purchased from Thermo Scientific) were gently inverted several times to disperse the microspheres and then immersed in an ultrasonic bath at 45 Hz. Two droplets of the 1 % microsphere suspension were further suspended in 250 ml deionized water (Millipore Alpha-Q, resistivity 18 M $\Omega$ cm) and stirred gently. A TEM formvar grid was placed on a 0.8  $\mu$ m pore size Millipore filter (type AA), which was lying upon a nutrient pad (the porous filter material used to hold nutrients in bacterial cultures) in contact with deionized water. 2  $\mu$ L of the microsphere suspension were placed on the surface of the grid with a hypodermic syringe. The grid, filters and water were kept in a fume hood for 24 h to allow the water and soluble material to diffuse through the plastic film into the water phase. The grid was subsequently stored in a desiccator until further SEM imaging.

## 4.2 Sizing results

The measured values for the diameters of the PSL particles were in the range of the manufacturer's size specifications; for the  $21 \pm 1$  nm spheres a diameter of 22.5 nm with a standard deviation of  $\pm 4.1$  nm was measured. The larger spheres showed successively smaller relative standard deviations:  $42.7 \pm 4.1$  nm,  $60.8 \pm 4.5$  nm,  $81.9 \pm 4.6$  nm,  $199.7 \pm 5.2$  nm and  $903.9 \pm 13.1$  nm (see Table 1). Generally the diameter for each of the PSL sphere sizes shows a good agreement with the size the manufacturer states in the NIST certificate following with each PSL sphere size: the number size distributions obtained for the PSL spheres are shown in Fig. 6, and examples for intensity histograms are shown in Fig. 7. The size distributions obtained from SEM imaging are monomodal with median values and standard deviations listed in Table 1. The magnitude of the relative standard deviation in our measurements decreased with the increase of the sphere diameter, from 18 % for the 20 nm spheres to 1.3 % for the 900 nm spheres. The same trend was observed for the elongation and circularity of the spheres, as these values

## A method for sizing submicrometer particles in air

E. Hamacher-Barth et al.

Title Page

Abstract

Introduction

Conclusions

References

Tables

Figures

◀

▶

◀

▶

Back

Close

Full Screen / Esc

Printer-friendly Version

Interactive Discussion



decrease continuously from 16 % deviation from the elongation for a perfect sphere for the 20 nm spheres to 0.13 % deviation for the 900 nm spheres. The values for circularity reveal measurements of spheres closer to the value of ideal circularity for a perfect sphere for the 900 nm spheres (0.2 % deviation) rather than for the 20 nm spheres (7 % deviation), see Table 1.

### 4.3 Determination of size limit of detection

At a magnification of 40000× the size of each pixel in the digital images is 2 nm and by assuming that the electron beam diameter is optimized with respect to focus and stigmatism, a diameter of 1 nm will be obtained. Under this condition the observed size limit of detection in the images will be about 5–10 nm in diameter. By use of 3 × 3 pixels to define a particle from the background noise in the Digital Image Analysis the theoretical minimum size of detection will then be particles with a diameter of 6 nm. At lower magnification the image pixel size and thus particle size that is possible to determine, increases. At 10000× the pixel size is 8 nm and the theoretical minimum size is 24 nm.

The real size limitation of detection of a particle also depends on the element composition of both particle and substrate, and the magnitude of accelerating voltage that generates the electron beam interaction volume. Summarizing the contributing factors the size limit of detection using the PSL particles was found to be around 15 nm by using a magnification of 40000×.

## 5 Airborne aerosol samples imaged by scanning electron microscope

Within the Arctic pack ice region studies of atmospheric aerosol composition resolved over size are sparse. The in-situ data archives include essentially only the observations of ASCOS and three previous research expeditions onboard the Swedish icebreaker *Oden* in the summers of 1991 (Leck et al., 1996c, 2001, 2004; Tjernström et al., 2004).

## A method for sizing submicrometer particles in air

E. Hamacher-Barth et al.

Title Page

Abstract

Introduction

Conclusions

References

Tables

Figures



Back

Close

Full Screen / Esc

Printer-friendly Version

Interactive Discussion



## A method for sizing submicrometer particles in air

E. Hamacher-Barth et al.

Title Page

Abstract

Introduction

Conclusions

References

Tables

Figures

◀

▶

◀

▶

Back

Close

Full Screen / Esc

Printer-friendly Version

Interactive Discussion



Based on the above efforts we have arrived at the following knowledge concerning the high Arctic aerosol sources and transformation while airborne: in summer the air in the Arctic is generally very clean and aerosol numbers are low (ca.  $100 \text{ cm}^{-3}$ ) because the air mass transport from strong mid-latitudinal polluted regions into the Arctic is reduced (Lannefors et al., 1983; Leck et al., 1996c; Heintzenberg et al., 2006). Nevertheless, during the four expeditions, the size distribution of aerosol particles have shown high variability, but generally presented itself as a superposition of more or less distinguishable modes (Covert et al., 1996; Heintzenberg and Leck, 2012). Following the original work of Whitby (1978) and Hoppel (1988) each of these modes can be represented by a log-normal distribution. Particles with sizes less than 10 nm diameter are generally rarely observed over remote oceans of temperate and tropic climates (Heintzenberg et al., 2004), but occasionally may suddenly increase dramatically for a brief period. In contrast to the warmer oceans, new particle formation events in the boundary layer (BL) of the central Arctic Ocean are relatively common during summer (Wiedensohler et al., 1996; Leck and Bigg, 1999; Leck and Bigg, 2010). At  $D > 10 \text{ nm}$  number concentrations increase up to a maximum somewhere between 25 nm and 80 nm, depending on the location (Heintzenberg and Leck, 2012; Kerminen and Leck, 2001; Leck and Bigg, 2005a, b). This so called Aitken mode results from condensation on, and self-coagulation of nucleation mode particles as well as from primary marine emissions (Leck and Bigg, 2010; Orellana et al., 2011). A concentration minimum, referred to as the Hoppel minimum, follows at about 80 nm. Another maximum, the so called the accumulation mode, occurs at about 100–200 nm. One further maximum appears at diameters larger than 1000 nm (the “coarse mode”), often inconspicuous in a number distribution but contributing substantially to aerosol volume/mass. The accumulation mode typically results from condensation of gases such as the oxidation products of dimethyl sulfide (sulfuric and- methane sulfonic acids), on pre-existing Aitken mode particles (Karl et al., 2012; Kerminen and Leck, 2001) and from the formation of particle mass by in-cloud chemistry via sulfur dioxide. In addition to creation of accumulation mode particles through growth processes, primary particles can be directly injected into

## A method for sizing submicrometer particles in air

E. Hamacher-Barth et al.

Title Page

Abstract

Introduction

Conclusions

References

Tables

Figures

◀

▶

◀

▶

Back

Close

Full Screen / Esc

Printer-friendly Version

Interactive Discussion



this mode by bubble bursting at the sea–air interface (Bigg and Leck, 2008; Leck and Bigg, 2005a; Leck et al., 2002). Over the summer pack ice near surface wind speeds are typically low ( $< \sim 6 \text{ ms}^{-1}$ ; Tjernström et al., 2012), and the extent of open water in leads in the pack ice is usually modest (10–30 %) so that fetches are short and the generation of waves is limited. In spite of the low winds a study performed during ASCOS confirmed both the presence and temporal variability of a population of bubbles within the open leads, and a non-wave bubble source mechanism, subsequently generating both film and jet drops, driven by the surface heat flux was proposed (Norris et al., 2011). However, past transmission electron microscope studies of individual particles by Bigg and Leck (2001a, 2008); Leck et al. (2002); Leck and Bigg (2005a,b) over the pack ice have failed to find evidence of sea salt particles  $< 200 \text{ nm}$  in diameter. To explain this lack of accumulation mode sea salt particles with a diameter less than  $200 \text{ nm}$  the same authors proposed a bubble-induced mechanism responsible for transporting polymer colloids and their gel-rich material (called marine gels) from the bulk seawater into the open lead surface microlayer ( $< 1000 \mu\text{m}$  thick at the air–sea interface). Orellana et al. (2011) have recently shown that polymeric marine gels originating from open leads are present in airborne aerosol particles in the high Arctic. Marine gels are physical gels (Verdugo, 2012) mainly built up by polysaccharide chains of dissolved organic carbon (DOC) and amino acids (Gao et al., 2011; McCarthy, 1996) that assemble/disassemble spontaneously and are held together by hydrophobic and ionic interactions with mainly  $\text{Ca}^{2+}$  as a counter-ion. Leck and Bigg (2005a,b) tested predominantly airborne sulfate (derived from dimethyl sulfide) particles for the presence of microgels. They detected marine gel material that acted as sites for condensation of volatile organic vapours in half or more of their samples.

### 5.1 The approach applied to two aerosol samples collected during ASCOS

The first sample (Sample A) was collected from 15 August, 15:55 to 22:46 UTC (total sampling time of 6:51 h). This period was dominated by air masses originating from the

## A method for sizing submicrometer particles in air

E. Hamacher-Barth et al.

Title Page

Abstract

Introduction

Conclusions

References

Tables

Figures

◀

▶

◀

▶

Back

Close

Full Screen / Esc

Printer-friendly Version

Interactive Discussion



Greenland and Barents Sea area<sup>1</sup> (see Fig. 8, left hand panel). The second sampling period (Sample B, 19 August from 8:20 until 16:46 UTC) was dominated by air advected from the Kara Sea (see Fig. 8, right hand panel). The total sampling time was 8:26 h. Both samples were collected at about 87° N but with different times spent over ice since the last contact with open sea. Days over ice (DOI)<sup>2</sup> were determined to be 0.9 days for Sample A and 4.5 days for Sample B.

The bimodal size distribution shown in Figs. 13 and 14 was observed for both samples following the characteristic of an aerosol in being modified by cloud processing (Hoppel, 1994) and suggests an aerosol source from the marginal ice zone (MIZ) and/or open water south thereof. This is consistent with the air mass back trajectory clusters showing the origin of the air masses reaching the position of the icebreaker at the respective sampling date (see Fig. 8). The bimodal distributions are based on previous findings (Bigg and Leck, 2008; Leck and Persson, 1996a,b; Leck and Bigg, 2005a, b; Leck et al., 2002) then likely to have been a result from both primary (marine gels) and secondary (dimethyl sulfide oxidation products, condensational growth and in-cloud oxidation) generated aerosol, within the open leads via bubble bursting between the pack ice and/or along the MIZ.

<sup>1</sup> 10 days backward trajectories for the air mass arriving at 100 m altitude at the position of the icebreaker. The Hybrid Single Particle Lagrangian Integrated Trajectory Model (HYSPPLIT) (Draxler and Rolph, 2011; Rolph, 2011) was used for the trajectory calculations based on data from the Global Data Assimilation System (GDAS) of the National Weather Service's National Centers for Environmental Prediction (NCEP).

<sup>2</sup> The time spent over the pack ice by the air mass since last contact with open sea (DOI) was calculated for the purposes of ASCOS as in Nilsson (1996) and uses the HYSPLIT back trajectories in combination with maps of sea ice distribution. The latter were created based on data from NSIDC, Boulder, United States, obtained by the sensor onboard the Aqua satellite, with the final analysis being conducted at the University of Bremen, Germany. The measure of DOI represents thus a simple parameter to summarize the evolution of the aerosol particles as a function of the synoptic scale systems since their last contact with open sea.

What has been clearly shown from the high Arctic campaigns is that the ambient collected aerosol particles are not necessarily spherical but can show a very irregular shape and surface (e.g. Bigg and Leck, 2001). Common to both Sample A and B we observe three types of particles:

5 – *Single particles (SP)*: these particles consist of single entities with a homogeneously distributed pixel intensity across the whole particle. They often contrast sharply and are relatively easy to separate from their background; for an example see Fig. 9. SP can be observed in the Aitken as well as in the accumulation mode size range. The single particles in the accumulation mode often collapse under the electron beam but keep their outer shape, which is typical for ammonium sulfate particles (Heard and Wiffen, 1969); for an example see Fig. 10. To avoid biases due to size changes, however, we imaged these particles as quickly as possible in order to minimize evaporative losses and beam damage, and at the same time optimize the contrast and surface information of the aerosol particles.

10 – *Gel particles (GP)*: in contrast to SP these particles show a patchy, inhomogeneous distribution of pixel intensity, for an example see Fig. 11. This patchy appearance and the partly very weak contrast against the formvar film suggest that these particles are built up by material that consists predominantly of light elements (C, H, N, O) and forms a film-like structure on the formvar film. The majority of GP appears in the accumulation mode.

15 Due to the nature of binding interactions between the divalent ions and the polysaccharide chains, gel particles easily undergo volume phase changes because of changes of temperature, pressure or pH (Verdugo et al., 2010). It thus might be possible that the gel material is destabilized, at least partly, through the impaction of the gel onto the formvar film. This destabilization can lead to a decrease in density and the formation of partly very weakly contrasting, film-like material on the formvar film. Being screened by the SEM this finally can lead to an underestimation of the area of the GP deposited on the film surface.

## A method for sizing submicrometer particles in air

E. Hamacher-Barth et al.

Title Page

Abstract

Introduction

Conclusions

References

Tables

Figures



Back

Close

Full Screen / Esc

Printer-friendly Version

Interactive Discussion



## A method for sizing submicrometer particles in air

E. Hamacher-Barth et al.

Title Page

Abstract

Introduction

Conclusions

References

Tables

Figures

◀

▶

◀

▶

Back

Close

Full Screen / Esc

Printer-friendly Version

Interactive Discussion



– *Halo particles (HP)*: a relatively large central particle is surrounded by a number of smaller satellite particles with  $D_{pa}/10$  to  $D_{pa}/3$  ( $D_{pa}$ : equivalent diameters derived from the area of the projected particle of the central particle using Eq. 1). Figure 12 shows an example. We estimate that satellite particles can contribute to up to 45 % to the  $D_{pa}$ . This estimate was obtained by manually determining the area (in pixel) of the central particle and the surrounding satellite particles on an image. By summing up these areas, the diameter of the hypothetically intact particle before splashing out on the formavar film and the proportion of the satellite particles can be calculated. But the satellite particles are small and contrast very weakly; thus they are difficult to capture with image processing. The latter biases the overall particle diameters of HP with a satellite type appearance towards smaller values and might contribute to the observed difference of the accumulation mode number maximum in peak positions in the SEM and TDMPS derived size distributions (see discussion of Sample A and B below).

As a consequence of the very different character and partly irregular appearance observed in the collected particles the determination of only their size does not capture comprehensive information about the aerosol particles. Thus we use morphological parameters for further characterization. All three types of particles described above were investigated separately and the morphological descriptors elongation and circularity were determined for each type of particle in each sample.

Moreover, to determine the uncertainty of our measurements we refer to the results from both the number distribution as a function of equivalent diameters derived from the area of the projected particle ( $D_{pa}$ ) based on the microscope technique and subsequent image mapping and the number distribution as a function of mobility diameters ( $D_m$ ) based on the TDMPS data. The underlying assumption for both independent methods is that the determined particles are spherical. The air sampled is in either case charged with the same  $^{63}\text{Ni}$ -emitting radioactive source. Both methods were calibrated against NIST traceable calibration standards of polystyrene latex spherical particles. The precision for the TDMA was determined to be less than 5 % independent of size (W. Birmili,

personal communication, 2013) and for the microscope determinations ranging from 18 % for sizes less than 20 nm to 1.3 % for 900 nm spheres (Table 1). The precision determined for the TDMA in use during ASCOS was a slightly lower than that reported by Mullholland et al. (2006): a 2 % deviation between SEM and TDMP5S measurements were determined for 100 nm PSL spheres. The authors assumed that this deviation increases with decreasing diameters of the PSL spheres.

Additionally for non-spherical particles  $D_m$  is a function of particle shape and orientation (DeCarlo et al., 2004). Nevertheless, previous studies from other authors (Rogak et al., 1993; Park et al., 2004) on diesel particles,  $\text{TiO}_2$  and Si particles have shown for non-spherical particles below 400 nm that  $D_m \sim D_{pa}$ . We thus can assume that the diameters obtained from TDMP5S and SEM imaging in our measurements are directly comparable and the error in the TDMP5S measurements due to non-sphericity of any aerosol particles can be neglected.

### 5.1.1 Discussion of Sample A

The SEM derived aerosol size distribution for Sample A (Fig. 13, red line) shows number maxima in the Aitken mode at 42 nm and at 109 nm diameters in the accumulation mode. The simultaneous TDMP5S measurement (Fig. 13, blue line) shows corresponding peaks at 34 nm and 133 nm diameters, respectively. The size determination of PSL spheres in the Aitken mode region that revealed a standard deviation of 4.1 nm (18 %) for 21 nm spheres and 4.1 nm (9.5 %) for 40 nm spheres (see Table 1), we assume a standard deviation of ca. 14 % for natural aerosol particles in the Aitken mode, and an at least 5 % uncertainty for the TDMP5S measurements (W. Birmili, personal communication, 2013). Considering these values we conclude that the position of the Aitken mode peaks for the SEM and TDMP5S derived diameters, 42 nm resp. 34 nm, lie within the statistical range of uncertainty determined for particles in this size range.

The accumulation mode for the SEM derived number maximum at 109 nm probably corresponds to the TDMP5S peak at 113 nm. Using the standard deviation of the PSL sphere diameters in this size range we can assume ca. 5 % uncertainty for the

## A method for sizing submicrometer particles in air

E. Hamacher-Barth et al.

Title Page

Abstract

Introduction

Conclusions

References

Tables

Figures



Back

Close

Full Screen / Esc

Printer-friendly Version

Interactive Discussion



aerosol particles in the accumulation mode for SEM derived diameters. Thus we conclude that the position of the accumulation mode peaks for both, SEM and TDMPs measurements at 109 and 133 nm, do not lie within the statistical range of uncertainty determined for particles within this size range (see Fig. 13).

The differences in peak positions, however, suggest that the particles occurring at 133 nm in the TDMPs size distribution are partly underestimated in the SEM measurements and their diameters are shifted towards the maximum at 109 nm.

To improve the understanding of the observed size distribution and to explore the causes for the observed shift in the accumulation mode peak position we determined the morphological parameters elongation and circularity of the observed particle types (see Table 2).

- *Single particles (SP)* appear in the 30–300 nm diameter size range and show a mean elongation of 0.334 and a mean circularity of 0.845. They comprise 85 % of the imaged particles.
- *Gel particles (GP)* appear mainly in the 70–322 nm diameter size range with a mean elongation of 0.639 and a circularity of 0.728. They contribute to about 10 % to the total particle number.
- *Halo particles (HP)* compose 5 % of the total particle number and are restricted to the accumulation mode region between 116–227 nm diameter. The central particles of the HP show a mean elongation of 0.140 and a circularity of 0.830.

Due to the particle properties and the observed shift in the accumulation mode it can be anticipated that the aerosol particles are partly underestimated due to their very weak contrast to the background, especially for GP, and the difficulty to quantitatively capture all satellite particles of the HP. The overall size distributions however show similar peak intensities and positions for both methods.

## A method for sizing submicrometer particles in air

E. Hamacher-Barth et al.

Title Page

Abstract

Introduction

Conclusions

References

Tables

Figures



Back

Close

Full Screen / Esc

Printer-friendly Version

Interactive Discussion



## 5.1.2 Discussion of Sample B

Imaged by SEM, Sample B shows aerosol number maxima at 47 nm in the Aitken mode and at 122 nm, with a shoulder at  $\sim 200$  nm, in the accumulation mode (Fig. 14, red line). The corresponding TDMPs measurements show number peaks in the Aitken mode at 52 nm and a peak at 166 nm diameters in the accumulation mode (Fig. 14, blue line). Assuming the same ranges of uncertainties as for Sample A the Aitken mode peaks show a good agreement of the peak positions in the SEM and TDMPs measurements, whereas the accumulation mode in SEM is shifted by 44 nm to smaller diameters compared to the TDMPs measurements and thus does not show any overlap with the peak position in SEM. Aerosol particles and their morphological parameters can be observed as follows:

- *Single particles (SP)* can be seen between 30–300 nm diameter and account for 85 % of the particle number. These particles type shows a mean elongation of 0.176 and a mean circularity of 0.670.
- *Gel particles (GP)* are observed between 70 and 530 nm diameter and show an elongation of 0.212 and a circularity of 0.165. They account for 10 % of all aerosol particles in sample B.
- *Halo particles (HP)* in the 50–230 nm diameter size range show an elongation of 0.090 and a mean circularity of 0.845 and account for 5 % of the total particle number.

As for Sample A we assumed that the aerosol particle diameters might be underestimated due to their partly very weak contrast to the background, as in the case for GP and satellite particles of HP. The overall size distribution, however, shows a bimodal peak pattern and similar peak intensities and positions for both methods.

## A method for sizing submicrometer particles in air

E. Hamacher-Barth et al.

Title Page

Abstract

Introduction

Conclusions

References

Tables

Figures

◀

▶

◀

▶

Back

Close

Full Screen / Esc

Printer-friendly Version

Interactive Discussion



## 5.2 Comparison of Sample A and Sample B

One of the most probable sources for aerosol particles is the surface water and specifically the surface micro-layer of the open water leads within the pack-ice region (Leck and Bigg, 2005a; Leck et al., 2002; Orellana et al., 2011). The subsequent transformation processes the aerosol particles undergo once they are airborne, e.g. through condensational vapours, are important since they affect the aerosol's ability to form cloud condensation nuclei (Bigg and Leck, 2001; Lohman and Leck, 2005; Martin et al., 2011). The size distributions and the morphological parameters reflect the impact of air mass transport on the aerosol particles and in the following we will compare Samples A and B with respect to them.

Aerosol particles observed in both samples have been collected from air masses that spent different times over the pack ice before reaching the icebreaker. Provided that the MIZ is a strong source of aerosol particles, a shorter DOI (0.9 days, Sample A) carrying freshly emitted airborne aerosol particles favors a strong Aitken mode whereas a longer DOI leads to a more pronounced accumulation mode (4.5 days, Sample B). Furthermore it can be noticed that the difference between SEM and TDMPs derived diameters for the accumulation mode of Sample B (44 nm difference, see Fig. 14) is much higher than for Sample A (24 nm difference, see Fig. 13). The latter might be caused by a higher degree of underestimation of the particle area for GP and satellite particles of HP in Sample B due to weakly contrasting material. Former work from Orellana and Verdugo (2003) showed that UV light destabilizes marine gels, and it might be possible that due to the longer DOI and thus a potentially longer exposure to UV light has lead to a weakening of the polymeric network and thus a decrease in density of the material that comprises the microgel in Sample B. We speculate that weakening of the polymeric network in marine gels through UV light might also lead to the generally higher diameters of the accumulation mode particles in Sample B (122 nm compared to 109 nm in Sample A).

# AMTD

6, 5401–5446, 2013

## A method for sizing submicrometer particles in air

E. Hamacher-Barth et al.

Title Page

Abstract

Introduction

Conclusions

References

Tables

Figures



Back

Close

Full Screen / Esc

Printer-friendly Version

Interactive Discussion



Simultaneously the morphological properties of the aerosol particles seem to change due to transport and transformation processes. Circularity and elongation are both measures of the roundness of a particle, but elongation is predominantly an indicator of the overall form of a particle whereas circularity is sensitive to both the overall form (like elongation) and surface roughness (via  $CP^2$ ; see above). Adding these parameters provides a more effective differentiator than a simple comparison of the size distributions of both samples.

– *Single particles (SP)*: mapped with SEM the SP show values for elongation and circularity (see Table 2) which indicate an overall shape that deviates more strongly from ideal sphericity for Sample A but particles with a rougher contour for the single particles mapped in Sample B:

– *Elongation*: with an elongation of 0.364 Sample A particles have a stronger elliptical component ( $D_{\max}: D_{\min} \approx 2.00 : 1$ ) as Sample B particles with an elongation of 0.176 ( $D_{\max}: D_{\min} \approx 1.42 : 1$ ).

– *Circularity*: SP in Sample A show a value for circularity of 0.845, whereas for sample B particles the value for circularity is 0.670. Calculating the values for CP for both samples reveals a 12 % larger value for  $CP_B$  with  $CP_B: CP_A = 1.12 : 1$ . The higher value for  $CP_B$  and thus a lower value for circularity for SP in Sample B indicate particles with a rougher contour compared to particles in Sample A.

– *Gel particles (GP)*: in SEM this type of aerosol particles shows a higher value for elongation in Sample A but particles with a higher deviation from ideal circularity and thus a rougher contour in sample B.

– *Elongation*: in Sample A the GP are to 18 % more elongated with a value of 0.639 and with  $D_{\max}: D_{\min} = 4.54$  compared to GP in Sample B where the elongation is 0.212 and the ratio of diameters is  $D_{\max}: D_{\min} = 1.54$ .

## A method for sizing submicrometer particles in air

E. Hamacher-Barth et al.

[Title Page](#)[Abstract](#)[Introduction](#)[Conclusions](#)[References](#)[Tables](#)[Figures](#)[⏪](#)[⏩](#)[◀](#)[▶](#)[Back](#)[Close](#)[Full Screen / Esc](#)[Printer-friendly Version](#)[Interactive Discussion](#)

## A method for sizing submicrometer particles in air

E. Hamacher-Barth et al.

Title Page

Abstract

Introduction

Conclusions

References

Tables

Figures



Back

Close

Full Screen / Esc

Printer-friendly Version

Interactive Discussion



- *Circularity*: GP in Sample B show a higher deviation from ideal circularity (circularity 0.165) compared to this type of particles in Sample A (circularity 0.728). The ratio of the Crofton Parameters is  $CP_A : CP_B = 2.10 : 1$  which indicates a much rougher surface for GP in Sample B compared to Sample A particles.
- *Halo particles (HP)*: the central particles exhibit almost no differences in morphology for both samples. Both samples show moderate degrees of elongation and deviations from ideal circularity that do not indicate any differences due to a change in DOI.
- *Elongation*: the central particles in Sample A show a value for elongation of 0.14 and thus are slightly more elongated than the central particles in Sample B (elongation 0.09). The ratio of diameters  $D_{\max} : D_{\min}$  is 1.33 : 1 for particles from Sample A, and  $D_{\max} : D_{\min} = 1.19 : 1$  for particles from Sample B.
- *Circularity*: the circularity shows values of 0.83 for central particles of Sample A and 0.845 for Sample B. The ratio of Crofton Perimeters is calculated to  $CP_A : CP_B = 1.008$  which indicates no significant differences in roughness for HP in both samples.

Examining the size distributions and morphological parameters for Sample A and Sample B reveals some important differences which, assuming that despite the geographically separated emission areas of for both samples (Barents- and Greenland Sea, respectively Kara Sea, see Fig. 8) the type of marine source is identical, might be connected to the different DOI of the air masses before reaching the ice breaker. For two types of aerosol particles (SP, GP) investigated in this study we observe a transition from stronger elongated and branched to more closed structures in course of increased DOI. The lower value in elongation for SP in Sample B could point towards a process that changes the particle shape to a rounder structure and is favored through a longer residence time in the atmosphere. The observed differences in circularity, however indicate changes of the particles towards a higher surface area (expressed by an increased

value for CP and a lower circularity) for GP and SP due to a higher DOI in Sample B. The surface of the particles did change towards a rougher contour, e.g. by condensation of vapours on the particle surface. Whether these morphological changes lead to changes in hygroscopicity and the incorporation of matter with surface-active properties, as it has been described for soot by Lehmann et al. (2006) and Coz and Leck (2011) has to be investigated in subsequent studies.

## 6 Conclusions

With our measurements we could show that SEM operating at low accelerating voltage (1 kV) and in GB modus provides a very accurate method to size aerosol particles collected on a TEM formvar grid without shading at an excellent resolution down to 20 nm diameter. The latter could be verified by measurement of certified PSL standard spheres and subsequent digital image analysis where the diameter values stated by the manufacturer could be reproduced with high accuracy and morphological parameters (elongation, circularity) were determined.

We applied our method to two samples of aerosol particles collected in the high Arctic during ASCOS 2008. Size distributions as well morphological parameters (elongation, circularity) were obtained for each sample. By comparing the size distributions with those from simultaneously performed TDMPs measurements we demonstrated that a representative fraction of the ambient aerosol was evaluated with the same bimodal characteristics as in TDMPs. The method of SEM/image mapping of individual particles presented above showed to be excellent in providing not only information of particle size but at the same time on particle morphology. The latter has shown to be very useful in providing information on possible aerosol transformation processes in air being advected over the pack ice.

However, imaging weakly contrasting species always bears the risk of underestimating the area of the projected particle with digital image processing, and we observe a shift of particle sizes to smaller diameters for particles in the accumulation mode that

## A method for sizing submicrometer particles in air

E. Hamacher-Barth et al.

Title Page

Abstract

Introduction

Conclusions

References

Tables

Figures



Back

Close

Full Screen / Esc

Printer-friendly Version

Interactive Discussion



## A method for sizing submicrometer particles in air

E. Hamacher-Barth et al.

Title Page

Abstract

Introduction

Conclusions

References

Tables

Figures

◀

▶

◀

▶

Back

Close

Full Screen / Esc

Printer-friendly Version

Interactive Discussion



are characterized by an inhomogeneous distribution of intensity across the particle area (GP) or appear as a large central particle surrounded by smaller satellite particles (HP). Particles with a homogeneous distribution of intensity on the digital image that contrast well against their background (SP) however show a good agreement in diameters with those measured by TDMPS.

*Acknowledgements.* This work is part of ASCOS (Arctic Summer Cloud Ocean Study) and was made possible by funding from the Swedish Research Council, the Knut and Alice Wallenberg Foundation and the DAMOCLES European Union 6th Framework Program Integrated Research Project. The Swedish Polar Research Secretariat (SPRS) provided access to the icebreaker *Oden* and logistical support. We are greatly indebted to the *Oden*'s Captain Matthias Peterson and his crew for invaluable assistance with all the logistical challenges. Michael Tjernström is specifically thanked for his co-coordination of ASCOS. ASCOS is an IPY project under the AICIA–IPY umbrella and an endorsed SOLAS project. The authors thank Andreas Held for collecting the particles during ASCOS 2008, and A. Öhrström and C. Rauschenberg for all their help with the sample imaging.

## References

- Allen, T.: Particle Size Measurement, Vol. 1, Chapman & Hall, London, 1997.
- Bigg, E. K. and Leck, C.: Cloud active particles over the central Arctic ocean, *J. Geophys. Res.*, 106, 32155–32166, 2001.
- Bigg, E. K. and Leck, C.: The composition of fragments of bubbles bursting at the ocean surface, *J. Geophys. Res.*, 113, D11209, doi:10.1029/2007JD009078, 2008.
- Bigg, E. K., Leck, C., and Tranvik, L.: Particulates of the surface microlayer of open water in the central Arctic Ocean in summer, *Mar. Chem.*, 91, 131–141, 2004.
- Capannelli, G., Castello, E., Comite, A., Costa, C., and Mamolini, G.: Electron microscopy characterization of airborne micro- and nanoparticulate matter, *J. Electron Microsc.*, 60, 117–131, 2011.
- Covert, D. S., Wiedensohler, A., Aalto, P., Heintzenberg, J., McMurry, P. H., and Leck, C.: Aerosol number size distributions from 3 to 500 nm diameter in the arctic marine boundary layer during summer and autumn, *Tellus B*, 48, 197–212, 1996.

**A method for sizing submicrometer particles in air**

E. Hamacher-Barth et al.

Title Page

Abstract

Introduction

Conclusions

References

Tables

Figures

◀

▶

◀

▶

Back

Close

Full Screen / Esc

Printer-friendly Version

Interactive Discussion



Coz, E. and Leck, C.: Morphology and state of mixture of atmospheric soot aggregates during the winter season over Southern Asia – a quantitative approach, *Tellus B*, 63, 107–116, 2011.

Coz, E., Artínano, B., Robinson, A. L., Casuccio, G. S., Lersch, T. L., and Pandis, S. N.: Individual particle morphology and acidity, *Aerosol Sci. Tech.*, 42, 224–232, 2008.

Crompton, C.: Particle Shape – An Important Factor in Pharmaceutical Manufacturing, PMPS, Spring issue, London, UK, 2005.

DeCarlo, P. F., Slowik, J. G., Worsnop, D. R., and Davidovits, P.: Particle morphology and density characterization by combined mobility and aerodynamic diameter measurements. Part 1: Theory, *Aerosol Sci. Tech.*, 38, 1185–1205, 2004.

Dixkens, J. and Fissan, H.: Development of an electrostatic precipitator for off-line particle analysis, *Aerosol Sci. Tech.*, 30, 438–453, 1999.

Draxler, R. R. and Rolph, G. D.: HYSPLIT (HYbrid Single-Particle Lagrangian Integrated Trajectory) Model, access via NOAA ARL READY Website, available at: <http://ready.arl.noaa.gov/HYSPLIT.php> (last access: 11 March 2013), NOAA Air Resources Laboratory, Silver Spring, MD, 2011.

Gao, Q., Nilsson, U., Ilag, L. L., and Leck, C.: Monosaccharide compositional analysis of marine polysaccharides by hydrophilic interaction liquid chromatography-tandem mass spectrometry, *Anal. Bioanal. Chem.*, 399, 2517–2529, 2011.

Heard, M. and Wiffen, R.: Electron microscopy of natural aerosols and the identification of particulate ammonium sulphate, *Atmos. Environ.*, 3, 337–340, 1969.

Heintzenberg, J. and Leck, C.: The summer aerosol in the central Arctic 1991–2008: did it change or not?, *Atmos. Chem. Phys.*, 12, 3969–3983, doi:10.5194/acp-12-3969-2012, 2012.

Heintzenberg, J., Birmili, W., Wiedensohler, A., Nowak, A., and Tuch, T.: Structure, variability and persistence of the submicrometre marine aerosol, *Tellus B*, 56, 357–367, 2004.

Heintzenberg, J., Leck, C., Birmili, W., Wehner, B., Tjernström, M., and Wiedensohler, A.: Aerosol number-size distributions during clear and fog periods in the summer high Arctic: 1991, 1996 and 2001, *Tellus B*, 58, 41–50, 2006.

Hinds, W.: *Aerosol Technology*, 2nd Edn., John Wiley & Sons, New York, 1999.

Hoppel, W. A., Frick, G. M., and Larson, R. E.: Effect of nonprecipitating clouds on the aerosol size distribution in the marine boundary layer, *Geophys. Res. Lett.*, 13, 125–128, 1986.

Huck, D.: Particle shape – an important parameter in pharmaceutical manufacturing, *Chem. Europe*, available at: <http://www.chemeurope.com> (last access: 24 April), 2013.

## A method for sizing submicrometer particles in air

E. Hamacher-Barth et al.

Title Page

Abstract

Introduction

Conclusions

References

Tables

Figures

◀

▶

◀

▶

Back

Close

Full Screen / Esc

Printer-friendly Version

Interactive Discussion



IPCC: Climate Change 2007: The Physical Science Basis, Contribution of Working Group I to the Fourth Assessment Report of the Intergovernmental Panel on Climate Change, edited by: Solomon, S., Qin, D., Manning, M., Chen, Z., Marquis, M., Averyt, K. B., Tignor, M., and Miller, H. L., Cambridge University Press, Cambridge, New York, 2007.

Junge, C.: Die Konstitution des atmosphärischen Aerosols, Annalen der Meteorologie, Beiheft, 1–15, 1952.

Kandler, K., Benker, N., Bundke, U., Cuevas, E., Ebert, M., Knippertz, P., Rodriguez, S., Schuetz, L., and Weinbruch, S.: Chemical composition and complex refractive index of Saharan Mineral Dust at Izana, Tenerife (Spain) derived by electron microscopy, Atmos. Environ., 41, 8058–8074, 2007.

Karl, M., Leck, C., Gross, A., and Pijola, L.: A study of new particle formation in the marine boundary layer over the central Arctic ocean using a flexible multi-component aerosol dynamic model, Tellus B, 64, 17158, doi:10.3402/tellusb.v64i0.17158, 2012.

Katoshevski, D., Nenes, A., and Seinfeld, J. H.: A study of processes that govern the maintenance of aerosols in the marine boundary layer, J. Aerosol Sci., 30, 503–532, 1999.

Kerminen, V. M. and Leck, C.: Sulfur chemistry over the central Arctic Ocean during the summer: gas-to-particle transformation, J. Geophys. Res., 106, 32087–32099, 2001.

Kulmala, M., Vehkamäki, H., Petäjä, T., Dal Maso, M., Lauri, A., Kerminen, V.-M., Birmili, W., and McMurry, P. H.: Formation and growth rates of ultrafine atmospheric particles: a review of observations, J. Aerosol Sci., 35, 143–176, 2004.

Lanefors, H., Heintzenberg, J., and Hansson, H.-C.: A comprehensive study of physical and chemical parameters of the Arctic summer aerosol; results from the Swedish expedition Ymer-80, Tellus B, 35, 40–54, 1983.

Laskin, A., Cowin, J., and Iedema, M.: Analysis of individual environmental particles using modern methods of electron microscopy and X-ray microanalysis, J. Electron Spectrosc., 150, 260–274, 2006.

Leck, C. and Bigg, E. K.: Aerosol production over remote marine areas – a new route, J. Geophys. Res., 26, 3577–3580, 1999.

Leck, C. and Bigg, E. K.: Biogenic particles in the surface microlayer and overlaying atmosphere in the central Arctic Ocean during summer, Tellus B, 57, 305–316, 2005a.

Leck, C. and Bigg, E. K.: Evolution of the marine aerosol – a new perspective, Geophys. Res. Lett., 32, L19803, doi:10.1029/2005GL023651, 2005b.

## A method for sizing submicrometer particles in air

E. Hamacher-Barth et al.

Title Page

Abstract

Introduction

Conclusions

References

Tables

Figures

◀

▶

◀

▶

Back

Close

Full Screen / Esc

Printer-friendly Version

Interactive Discussion



- Leck, C. and Bigg, E. K.: Comparison of sources and nature of the tropical aerosol with the summer high Arctic aerosol, *Tellus B*, 60, 118–126, 2008.
- Leck, C. and Bigg, E. K.: New particle formation of marine biological origin, *Aerosol Sci. Tech.*, 44, 570–577, 2010.
- 5 Leck, C. and Persson, C.: Seasonal and short-term variability in dimethyl sulfide, sulfur dioxide and biogenic sulfur and sea salt aerosol particles in the arctic marine boundary layer during summer and autumn, *Tellus B*, 48, 272–299, 1996a.
- Leck, C. and Persson, C.: The central Arctic Ocean as a source of dimethyl sulfide: seasonal variability in relation to biological activity, *Tellus B*, 48, 156–177, 1996b.
- 10 Leck, C., Bigg, E. K., Covert, D. S., Heintzenberg, J., Maenhaut, W., Nilsson, E. D., and Wiedensohler, A.: Overview of the atmospheric research program during the International Arctic Ocean Expedition 1991 (IAOE-91) and its scientific results, *Tellus B*, 48, 136–155, 1996.
- Leck, C., Nilsson, E. D., and Bäcklin, L.: The atmospheric program of the Arctic Ocean Expedition in the summer of 1996 (AOE-96) – a technical overview – outline of experimental approach, instruments, scientific objectives, *J. Geophys. Res.*, 106, 32051–32067, 2001.
- 15 Leck, C., Norman, M., Bigg, K. E., and Hillamo, R.: Chemical composition and sources of the high Arctic aerosol relevant for cloud formation, *J. Geophys. Res.*, 107, 1–17, 2002.
- Leck, C., Tjernström, M., Matrai, P., Swietlicki, E., and Bigg, E. K.: Can marine micro-organisms influence melting of the Arctic pack-ice?, *Eos*, 85, 25–36, 2004.
- 20 Lehmann, J., Gaunt, J., and Rodon, M.: Bio-char sequestration in terrestrial ecosystems – a review, *Mitigation and Adaptation Strategies for Global Change*, 11, 403–427, 2006.
- Lohmann, U. and Leck, C.: Importance of submicron surface active organic aerosols for pristine Arctic clouds, *Tellus B*, 57, 261–268, 2005.
- Martin, M., Chang, R. Y.-W., Sierau, B., Sjogren, S., Swietlicki, E., Abbatt, J. P. D., Leck, C., and Lohmann, U.: Cloud condensation nuclei closure study on summer arctic aerosol, *Atmos. Chem. Phys.*, 11, 11335–11350, doi:10.5194/acp-11-11335-2011, 2011.
- 25 McCarthy, M., Hedges, J., and Benner, R.: Major biochemical composition of dissolved high molecular weight organic matter in seawater, *Mar. Chem.*, 55, 281–297, 1996.
- Meyer, F.: Mathematical morphology: from two dimensions to three dimensions, *J. Microsc.*, 165, 5–28, 1992.
- 30 Mullholland, G. W., Donnelly, M. K., Hagwood, C. R., Kukuck, S. R., and Hackley, V. A.: Measurement of 100 nm and 60 nm particle standards by differential mobility analysis, *J. Res. Natl. Inst. Stan.*, 111, 257–312, 2006.

## A method for sizing submicrometer particles in air

E. Hamacher-Barth et al.

Title Page

Abstract

Introduction

Conclusions

References

Tables

Figures

◀

▶

◀

▶

Back

Close

Full Screen / Esc

Printer-friendly Version

Interactive Discussion



Norris, S. J., Brooks, I. M., de Leeuw, G., Sirevaag, A., Leck, C., Brooks, B. J., Birch, C. E., and Tjernström, M.: Measurements of bubble size spectra within leads in the Arctic summer pack ice, *Ocean Sci.*, 7, 129–139, doi:10.5194/os-7-129-2011, 2011.

Orellana, M. V. and Verdugo, P.: Ultraviolet radiation blocks the organic carbon exchange between the dissolved phase and the gel phase in the ocean, *Limnol. Oceanogr.*, 48, 1618–1623, 2003.

Orellana, M. V., Matrai, P. A., Leck, C., Rauschenberg, C. D., Lee, A. M., and Coz, E.: Marine microgels as a source of cloud condensation nuclei in the high Arctic, *P. Natl. Acad. Sci. USA*, 108, 13612–13617, 2011.

Park, K., Kittelson, D. B., and McMurry, P. H.: Structural properties of diesel exhaust particles measured by transmission electron microscopy (TEM): relationships to particle mass and mobility, *Aerosol Sci. Tech.*, 38, 881–889, 2004.

Parungo, F. and Nagamoto, C.: Temporal and spatial variations of marine aerosols over the Atlantic Ocean, *Atmos. Res.*, 20, 23–37, 1986.

Rogak, S. N., Flagan, R. C., and Nguyen, H. V.: The mobility and structure of aerosol aggregates, *Aerosol Sci. Tech.*, 18, 25–47, 1993.

Rolph, G. D.: Real-time Environmental Applications and Display sYstem (READY) Website, available at: <http://ready.arl.noaa.gov> (last access: 11 March 2013), NOAA Air Resources Laboratory, Silver Spring, MD, 2011.

Serra, J.: *Image Analysis and Mathematical Morphology*, vol. 2, Theoretical Advances Academic Press, London, 309 pp., 1988.

Stevens, S. M., Jansson, K., Xiao, C., Asahina, S., Klingstedt, M., Grüner, D., Sakamoto, Y., Keiichi, M., Cubillas, P., Brent, R., Han, L., Che, S., Ryoo, R., Zhao, D., Anderson, M., Schüth, F., and Terasaki, O.: An appraisal of high resolution scanning electron microscopy to porous material, *JEOL news*, 44, 17–22, 2009.

Tjerström, M., Leck, C., Persson, P. O., Jensen, M., Oncley, S., and Targino, A.: The summer-time arctic atmosphere: meteorological measurements during the Arctic Ocean Experiment 2001 (AOE-2001), *B. Am. Meteorol. Soc.*, 85, 1305–1321, 2004.

Tjernström, M., Leck, C., Birch, C. E., Brooks, B. J., Brooks, I. M., Bäcklin, L., Chang, R. Y.-W., Granath, E., Graus, M., Hansel, A., Heintzenberg, J., Held, A., Hind, A., de la Rosa, S., Johnston, P., Knulst, J., de Leeuw, G., Di Liberto, L., Martin, M., Matrai, P. A., Mauritsen, T., Müller, M., Norris, S. J., Orellana, M. V., Orsini, D. A., Paatero, J., Persson, P. O. G., Gao, Q., Rauschenberg, C., Ristovski, Z., Sedlar, J., Shupe, M. D., Sierau, B., Sirevaag, A.,

Sjogren, S., Stetzer, O., Swietlicki, E., Szczodrak, M., Vaattovaara, P., Wahlberg, N., Westberg, M., and Wheeler, C. R.: The Arctic Summer Cloud-Ocean Study (ASCOS): overview and experimental design, *Atmos. Chem. Phys. Discuss.*, 13, 13541–13652, doi:10.5194/acpd-13-13541-2013, 2013.

5 Verdugo, P.: Marine microgels, *Annu. Rev. Mar. Sci.*, 4, 375–400, 2012.

Verdugo, P. and Santschi, P. H.: Polymer dynamics of DOC networks and gel formation in seawater, *Deep-Sea Res. Pt. II*, 52, 1483–1493, 2010.

10 Wiedensohler, A., Covert, D. A., Swietlicky, E. S., Aalto, P., and Heintzenberg, J.: Occurrence of an ultrafine particle mode less than 20 nm in diameter in the marine boundary layer during the Arctic summer, *Tellus B*, 48, 213–222, 1996.

Whitby, K. T.: The physical characteristics of sulfur aerosols, *Atmos. Environ.*, 12, 135–159, 1978.

## AMTD

6, 5401–5446, 2013

### A method for sizing submicrometer particles in air

E. Hamacher-Barth et al.

Title Page

Abstract

Introduction

Conclusions

References

Tables

Figures

◀

▶

◀

▶

Back

Close

Full Screen / Esc

Printer-friendly Version

Interactive Discussion



## A method for sizing submicrometer particles in air

E. Hamacher-Barth et al.

**Table 1.** Diameter and the morphological parameters, elongation and circularity, of PSL spheres derived by digital image analysis of SEM images at 40000 $\times$ . In brackets the relative magnitude of the standard deviation, the relative deviation from elongation and circularity of an ideal sphere.

	21 nm	40 nm	60 nm	80 nm	200 nm	900 nm
Certificate	21 $\pm$ 1 nm	40 $\pm$ 1 nm	57 $\pm$ 4 nm	81 $\pm$ 3 nm	200 $\pm$ 6 nm	903 $\pm$ 12 nm
Measured	22.5 $\pm$ 4.1 nm (18%)	42.7 $\pm$ 4.1 nm (9.5%)	60.8 $\pm$ 4.5 nm (7.3%)	81.9 $\pm$ 4.6 nm (5.6%)	199.7 $\pm$ 5.2 nm (2.6%)	903.9 $\pm$ 13.1 nm (1.4%)
Elongation (sphere = 0)	0.16 (16%)	0.09 (9%)	0.05 (5%)	0.04 (4%)	0.03 (3%)	0.001 (0.13%)
Circularity (sphere = 1)	0.93 (7%)	0.93 (7%)	0.94 (6%)	0.94 (6%)	0.97 (3%)	0.998 (0.2%)

Title Page

Abstract

Introduction

Conclusions

References

Tables

Figures

◀

▶

◀

▶

Back

Close

Full Screen / Esc

Printer-friendly Version

Interactive Discussion



## A method for sizing submicrometer particles in air

E. Hamacher-Barth et al.

Title Page

Abstract

Introduction

Conclusions

References

Tables

Figures

⏪

⏩

◀

▶

Back

Close

Full Screen / Esc

Printer-friendly Version

Interactive Discussion



**Table 2.** Morphological parameters elongation and circularity with size ranges for the observed particles types in samples A and B.

	Single particles (SP)			Halo particles (HP)			Gel particles (GP)		
	Size range	Elongation	Circularity	Size range	Elongation	Circularity	Size range	Elongation	Circularity
Sample A	30–300 nm	0.334 ± 0.08	0.845 ± 0.07	116–227 nm	0.14 ± 0.067	0.830 ± 0.08	70–322 nm	0.639 ± 0.077	0.728 ± 0.142
Sample B	30–300 nm	0.176 ± 0.090	0.670 ± 0.209	51–233 nm	0.090 ± 0.05	0.845 ± 0.067	70–532 nm	0.212 ± 0.089	0.165 ± 0.072

## A method for sizing submicrometer particles in air

E. Hamacher-Barth et al.

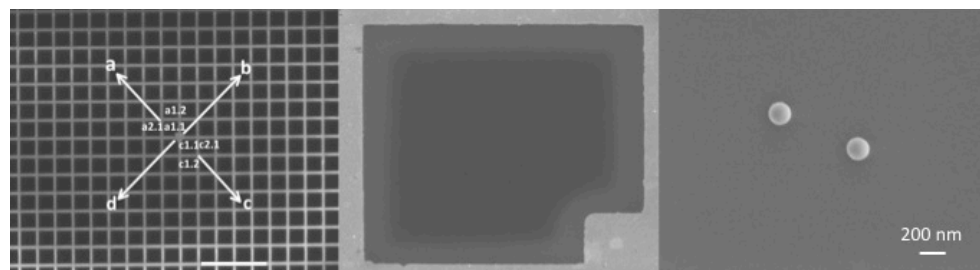


**Fig. 1.** (left) A copper grid imaged using SEM at 80× magnification showing the grid marker at centre and definition of the square labelling in quadrant a and c, (middle) the single grid square (a1,1) imaged at 1100× magnification, (right) particles imaged at 40 000× magnification.

[Title Page](#)[Abstract](#)[Introduction](#)[Conclusions](#)[References](#)[Tables](#)[Figures](#)[◀](#)[▶](#)[◀](#)[▶](#)[Back](#)[Close](#)[Full Screen / Esc](#)[Printer-friendly Version](#)[Interactive Discussion](#)

**A method for sizing  
submicrometer  
particles in air**

E. Hamacher-Barth et al.

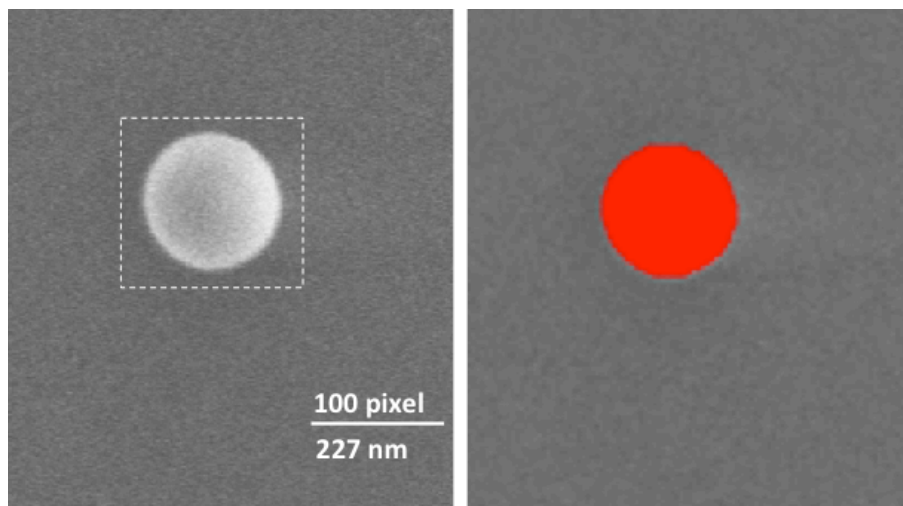


**Fig. 2.** Image for determination of the background intensity (left) and corresponding digital image used in measurement of particle size and morphological parameters (right).

[Title Page](#)[Abstract](#)[Introduction](#)[Conclusions](#)[References](#)[Tables](#)[Figures](#)[◀](#)[▶](#)[◀](#)[▶](#)[Back](#)[Close](#)[Full Screen / Esc](#)[Printer-friendly Version](#)[Interactive Discussion](#)

## A method for sizing submicrometer particles in air

E. Hamacher-Barth et al.

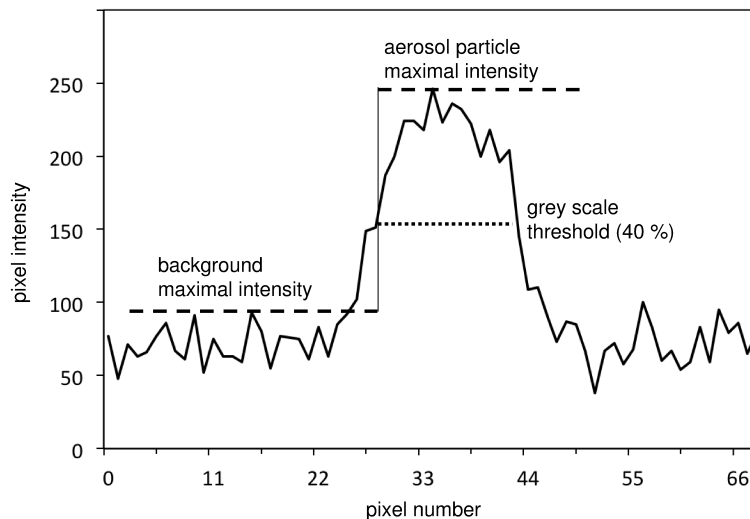


**Fig. 3.** Determination of aerosol particle size. Background and particle intensity were determined independently; the threshold for the determination of the particle size was set at 40 % of the intensity difference between background and aerosol particle maximal intensity.

[Title Page](#)[Abstract](#)[Introduction](#)[Conclusions](#)[References](#)[Tables](#)[Figures](#)[◀](#)[▶](#)[◀](#)[▶](#)[Back](#)[Close](#)[Full Screen / Esc](#)[Printer-friendly Version](#)[Interactive Discussion](#)

## A method for sizing submicrometer particles in air

E. Hamacher-Barth et al.

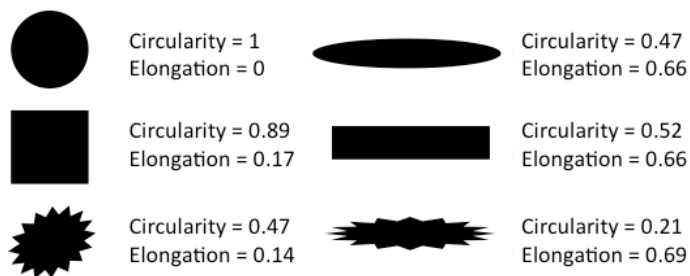


**Fig. 4.** Illustration of the morphological descriptors and elongation circularity (Huck, 2013, modified).

Title Page

Abstract

Introduction

Conclusions

References

Tables

Figures



Back

Close

Full Screen / Esc

Printer-friendly Version

Interactive Discussion



## A method for sizing submicrometer particles in air

E. Hamacher-Barth et al.

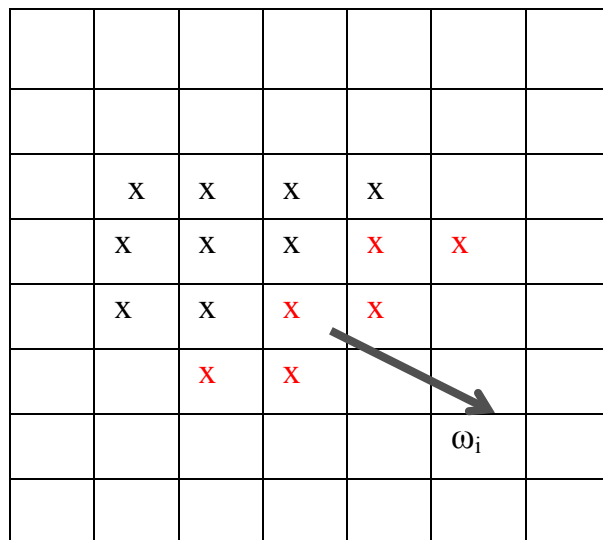


**Fig. 5.** Schematic representation of the calculation of the Crofton perimeter. The pixels with transitions from intensity to non-intensity are shown in red,  $\omega_i$  is the orientation along which the number of intercepts  $N_i$  are calculated.

Title Page

Abstract

Introduction

Conclusions

References

Tables

Figures

◀

▶

◀

▶

Back

Close

Full Screen / Esc

Printer-friendly Version

Interactive Discussion



## A method for sizing submicrometer particles in air

E. Hamacher-Barth et al.

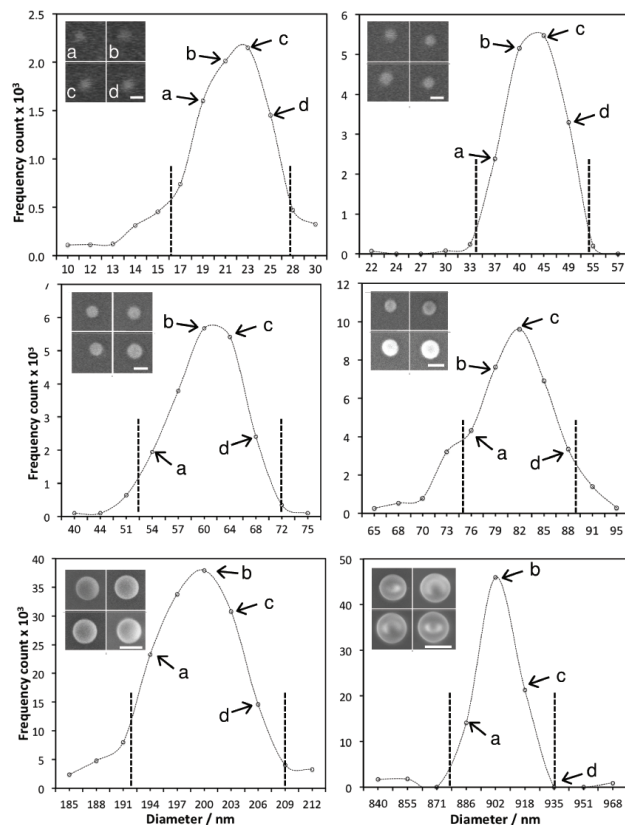


**Fig. 6.** Size distributions obtained for PSL spheres: 21 nm (upper left), 40 nm (upper right), 60 nm (middle left), 80 nm (middle right), 200 nm (lower right), and 900 nm (lower left). The dashed lines indicate the diameter boundary values for statistical analysis and the determination of morphological parameters. The insets show examples for the respective PSL spheres, and the calibration bars represent 20 nm (upper left), 40 nm (upper right), 60 nm (middle left), 80 nm (middle right), 200 nm (lower right), and 900 nm (lower left).

[Title Page](#)
[Abstract](#)
[Introduction](#)
[Conclusions](#)
[References](#)
[Tables](#)
[Figures](#)
[◀](#)
[▶](#)
[◀](#)
[▶](#)
[Back](#)
[Close](#)
[Full Screen / Esc](#)
[Printer-friendly Version](#)
[Interactive Discussion](#)


## A method for sizing submicrometer particles in air

E. Hamacher-Barth et al.

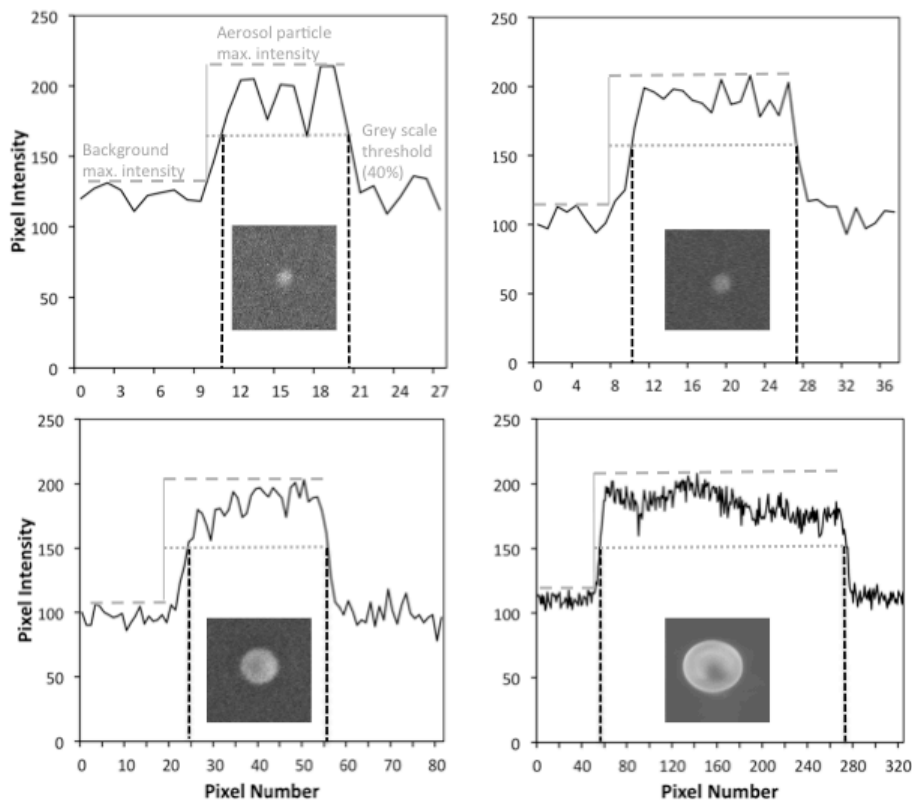


**Fig. 7.** Pixel intensities vs. pixel number for 20 nm PSL spheres (upper left), 40 nm PSL spheres (upper right), 80 nm PSL spheres (lower left) and 900 nm PSL spheres (lower right). The dashed lines indicate the boundaries for the determination of the background grey level threshold values.

Title Page

Abstract

Introduction

Conclusions

References

Tables

Figures

◀

▶

◀

▶

Back

Close

Full Screen / Esc

Printer-friendly Version

Interactive Discussion



**A method for sizing  
submicrometer  
particles in air**

E. Hamacher-Barth et al.

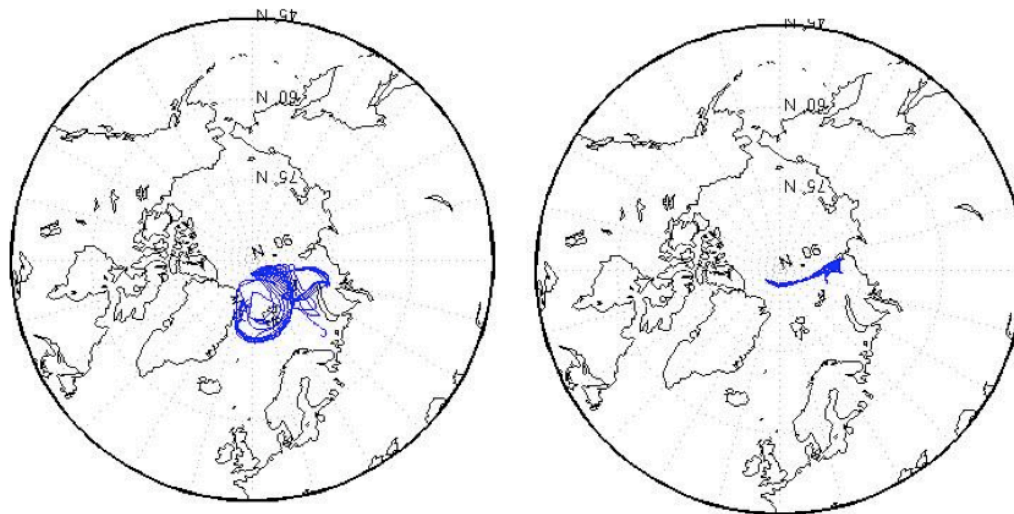


**Fig. 8.** Air mass trajectory clusters with an arrival height of 100 m at the position of the ice-breaker during: (left panel): 15 August originated easterly from the Greenland and Barents Sea area, (right panel): 19 August from the Kara Sea.

[Title Page](#)[Abstract](#)[Introduction](#)[Conclusions](#)[References](#)[Tables](#)[Figures](#)[◀](#)[▶](#)[◀](#)[▶](#)[Back](#)[Close](#)[Full Screen / Esc](#)[Printer-friendly Version](#)[Interactive Discussion](#)

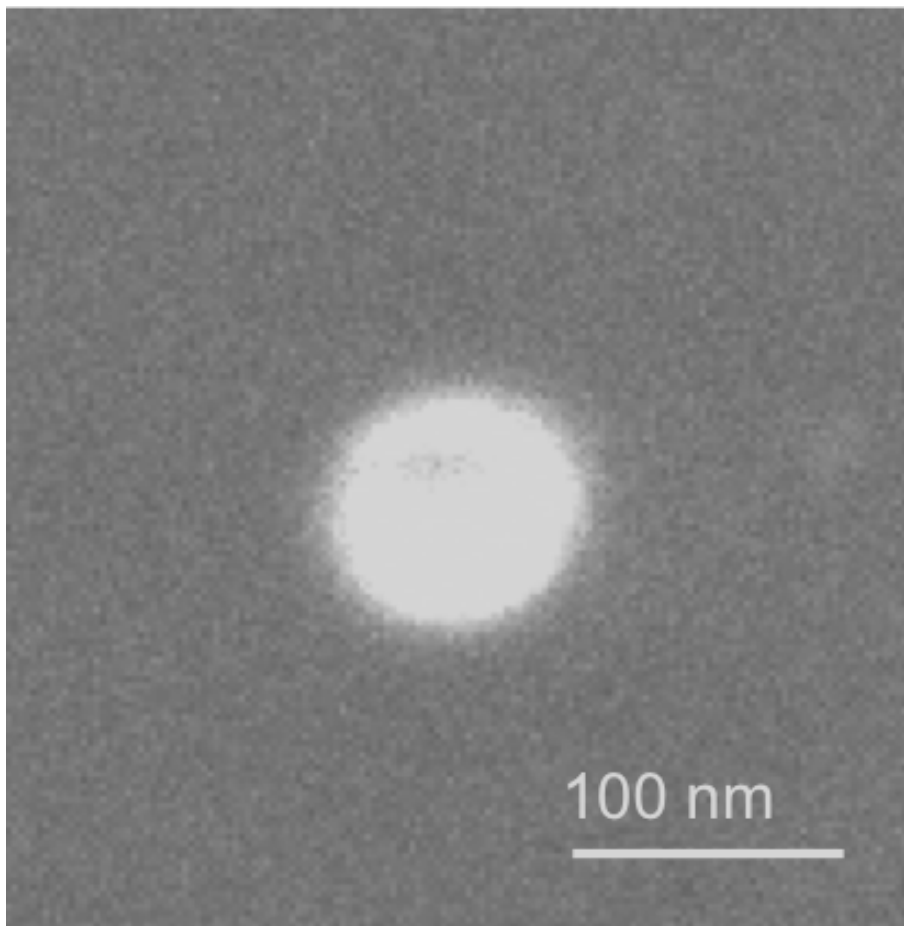


**Fig. 9.** An example for a single particle (SP) with a homogeneously distributed pixel intensity across the aerosol particle.

## AMTD

6, 5401–5446, 2013

### A method for sizing submicrometer particles in air

E. Hamacher-Barth et al.

Title Page

Abstract

Introduction

Conclusions

References

Tables

Figures

◀

▶

◀

▶

Back

Close

Full Screen / Esc

Printer-friendly Version

Interactive Discussion



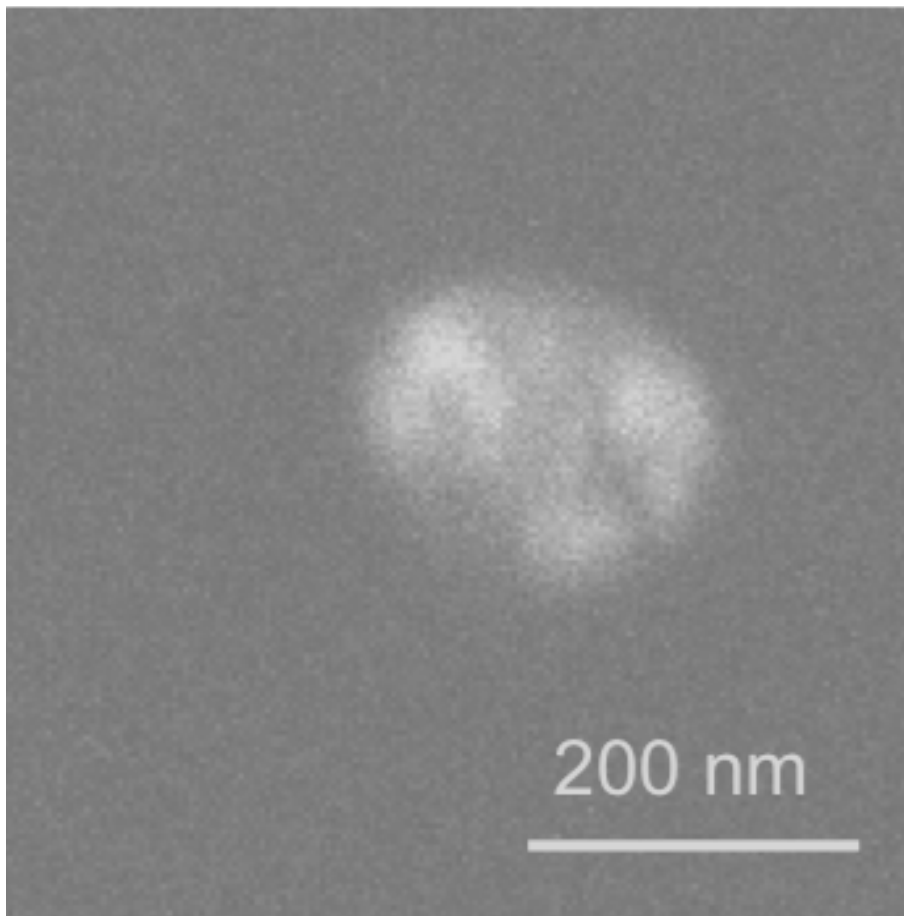


**Fig. 10.** An example for an ammonium sulfate particle which has partly collapsed under the electron beam but kept its outer shape.

## AMTD

6, 5401–5446, 2013

### A method for sizing submicrometer particles in air

E. Hamacher-Barth et al.

Title Page

Abstract

Introduction

Conclusions

References

Tables

Figures

◀

▶

◀

▶

Back

Close

Full Screen / Esc

Printer-friendly Version

Interactive Discussion



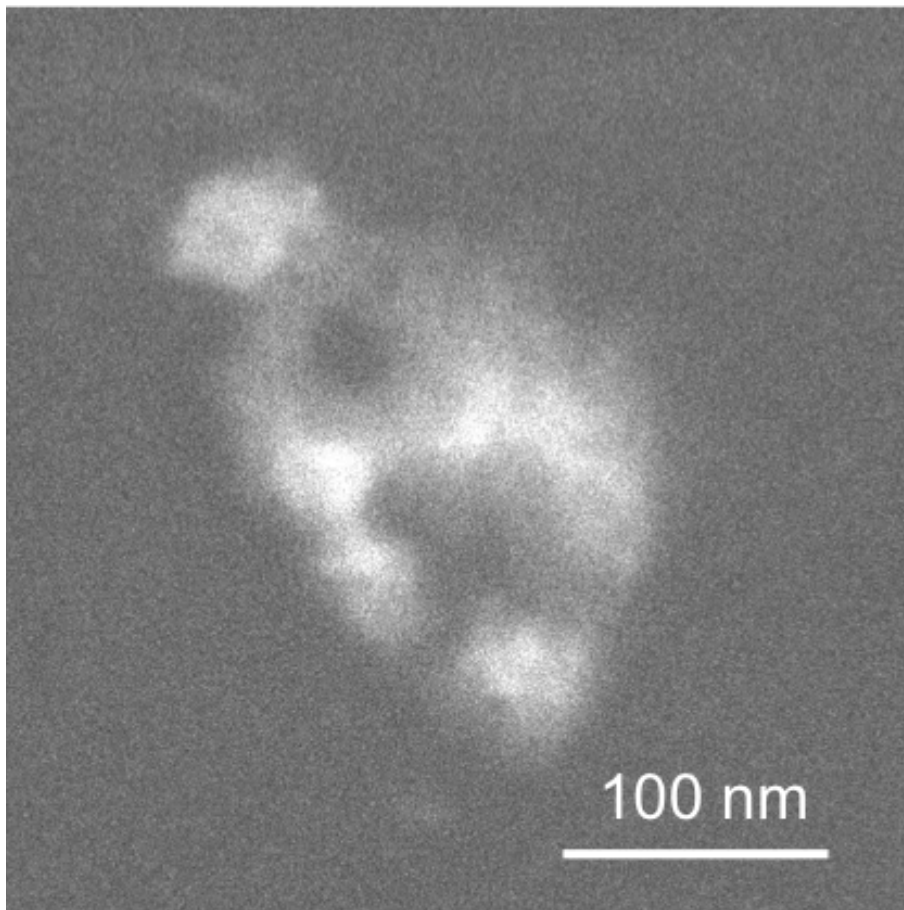


**Fig. 11.** An example for an aerosol particle with a patchy appearance and an inhomogeneous distribution of pixel intensity across the particle area (Gel particle, GP).

## A method for sizing submicrometer particles in air

E. Hamacher-Barth et al.

Title Page

Abstract

Introduction

Conclusions

References

Tables

Figures

◀

▶

◀

▶

Back

Close

Full Screen / Esc

Printer-friendly Version

Interactive Discussion



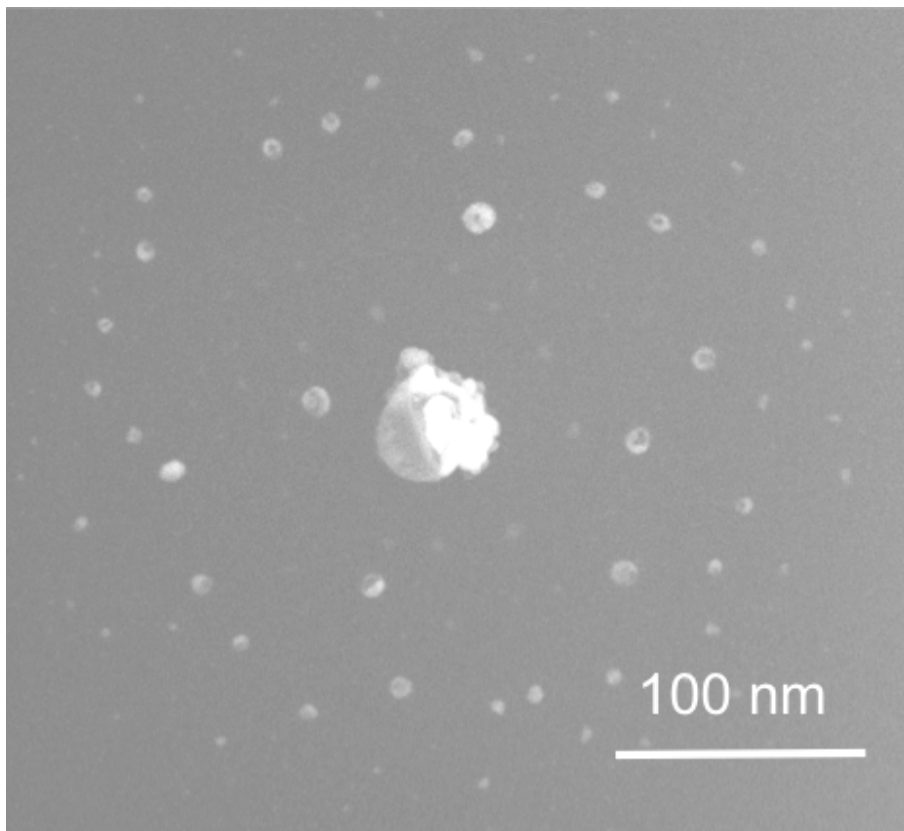


**Fig. 12.** An example for a satellite type structure of an aerosol particle (Halo particle, HP). When the aerosol particle impacts on the TEM formvar film it probably splashes out forming a number of small satellite particles surrounding a larger central core particle.

## A method for sizing submicrometer particles in air

E. Hamacher-Barth et al.

Title Page

Abstract

Introduction

Conclusions

References

Tables

Figures

◀

▶

◀

▶

Back

Close

Full Screen / Esc

Printer-friendly Version

Interactive Discussion



## A method for sizing submicrometer particles in air

E. Hamacher-Barth et al.

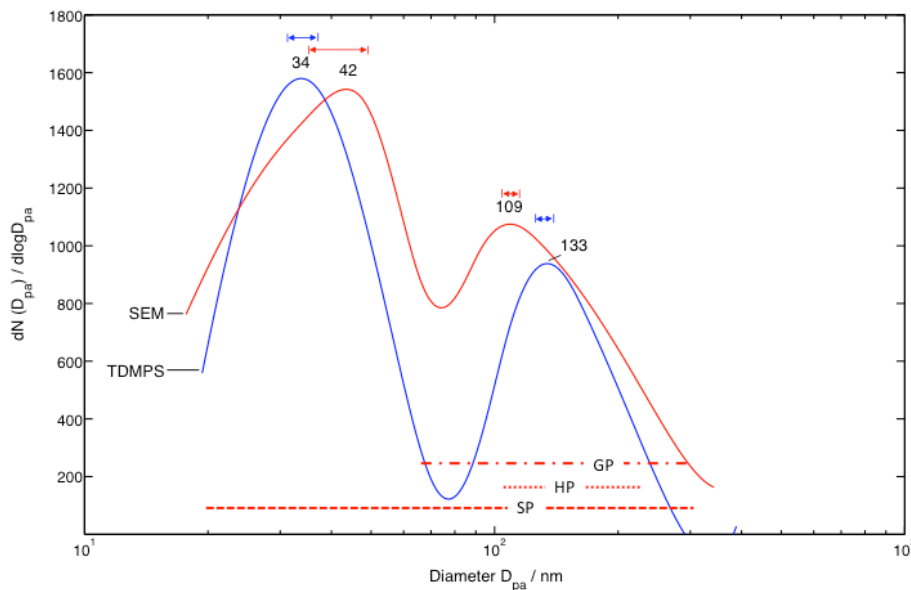


**Fig. 13.** Number size distributions obtained for sample A. Red line: SEM derived particle number distribution, blue line: number size distribution from TDMPS measurements. The red bars represent the size ranges in which particle types appear in SEM; SP: dashed line, HP: dotted line, GP: dash-dot line; the arrows represent the ranges of uncertainty for the respective mode in each size distribution based on results from sizing of PSL spheres for SEM data, and 5% uncertainty for TDMPS measurements (Birmili, personal communication, 2013).

Title Page

Abstract

Introduction

Conclusions

References

Tables

Figures

◀

▶

◀

▶

Back

Close

Full Screen / Esc

Printer-friendly Version

Interactive Discussion



## A method for sizing submicrometer particles in air

E. Hamacher-Barth et al.

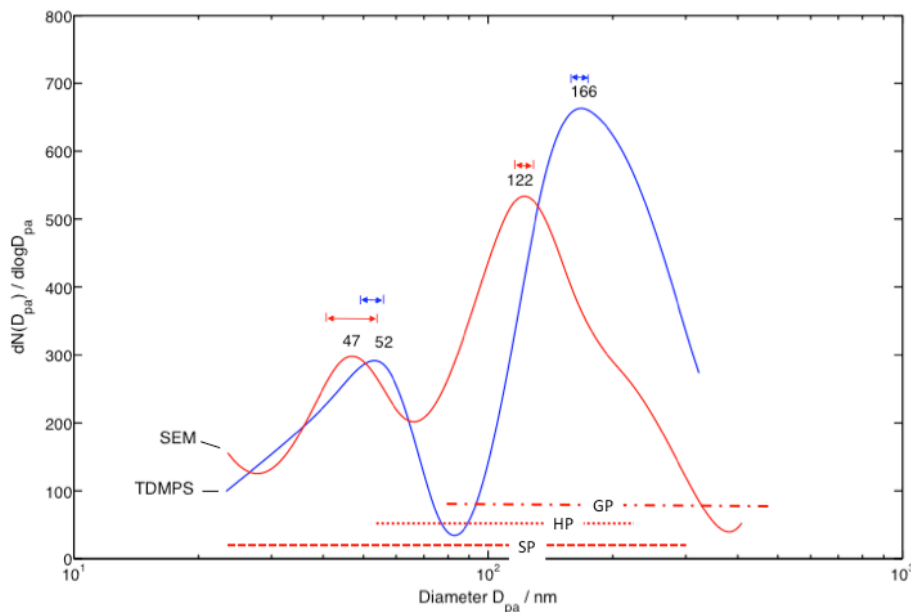


**Fig. 14.** Number size distribution obtained for sample B. Red line: SEM derived particle number distribution, blue line: number size distribution from TDMPS measurements. The red bars represent the size ranges in which particle types appear in SEM; SP: dashed line, HP: dotted line, GP: dash-dot line. The arrows represent the ranges of uncertainty for the respective mode in each size distribution based on results from sizing of PSL spheres for SEM data, and 5% uncertainty for TDMPS measurements (Birmili, personal communication, 2013).

Title Page

Abstract

Introduction

Conclusions

References

Tables

Figures

◀

▶

◀

▶

Back

Close

Full Screen / Esc

Printer-friendly Version

Interactive Discussion

